Elastic and damping characterization of open-pore metal foams filled or not with an elastomer for vibration control in turbomachinery

Endri Laçaj, Pascal Jolly, Jean Bouyer, Pascal Doumalin

Mechanics & Industry **25**, 23 (2024)
© E. Laçaj et al., Published by EDP Sciences 2024
https://doi.org/10.1051/meca/2024021

Mechanics & Industry

Available online at:
www.mechanics-industry.org

Regular Article

Open Access

Elastic and damping characterization of open-pore metal foams filled or not with an elastomer for vibration control in turbomachinery

Endri Laçaj, Pascal Jolly*, Jean Bouyer, and Pascal Doumalin

Institut Pprime, UPR CNRS 3346, Université de Poitiers, ISAE ENSMA, 86360 Chasseneuil du Poitou, France

Received: 28 November 2023 / Accepted: 21 July 2024

Abstract. In this work, an experimental investigation into vibration damping of elastomer filled open-pore metal foams and their effectiveness as a bearing support in turbomachinery is presented. The polyurethane fillers known for their high-energy absorption capacity were chosen to enhance the damping performance of the metal skeleton. Aluminum (Al), copper (Cu) and nickel-chromium foams (NiCr), with different relative density and pore size were tested dynamically using a dedicated device based on a single degree-of-freedom model. The results indicate that the storage modulus and the loss factor for foam-polymer composites were greater than the combined contribution of both phases taken separately. Foam morphology plays an important role in this effect and it is shown that the increase in performance was more significant for higher specific surface area. Fillers with different properties were also considered. The optimal combination of foam and polymer was selected and tested on a rotor kit test bench. Annular shaped samples were placed between the external race of the ball bearing and the housing. The tests were carried out using a flexible rotor configuration where the vibration amplitudes of the rotor were monitored for foam and foam-polyurethane composites for rotational speeds up to 100 Hz while hammer impact tests were performed using a semi-rigid shaft configuration due to higher resonance frequencies. In the first case, no significant difference was observed between the foam, foam composite and the bearings-only set-up. In the second case, the foam composite resulted with the highest energy dissipation capacity.

Keywords: Metal-foam / elastomer composites / bearings / vibration damping / turbomachinery

1 Introduction

During their operation, rotating machines are susceptible to dynamic loads that cause undesired vibrations and shocks if not controlled properly. The support elements play an important role in limiting these effects and guaranteeing safe running conditions by providing optimal stiffness and damping into the system. In various applications, among which aerospace, squeeze film dampers (SFD) have been effectively used to reduce the vibratory response coming from residual unbalance on the rotor. But their disadvantages are the clutter, usage of pressurized oil, and the presence of a squirrel cage. Moreover, this device cannot avoid the aging of the fluid and tuning which is needed for compensating the temperature and frequency effects. Hence, finding new technical solutions that guarantee load support, vibration damping as well as an oil free operation remains an active research area. In this regard, similar motivations have led to the employment of new materials like metal rubbers, combining an elastic structure with high energy dissipating capabilities from its internal friction [1,2]. Due to their porous structure, further improvement on these properties could be achieved by impregnating them with polymer fillers [3]. However, due to its internal configuration, the material stiffness is prone to variations with time [4] and may require additional springs, increasing their complexity and weight [5,6]. Metal and ceramic open-cell foams with their connected microstructure on the other hand, offer better structural integrity and high stiffness to weight ratio. These foams itself have low damping as their base constituents but, due to their open pores they can be filled with elastomers to obtain composites with an attractive combination of properties, inheriting the stiffness and load carrying capacity of its metallic/ceramic phase and the energy dissipating mechanisms of elastomer fillers or interactions between the phases.

It is common for these porous materials to be impregnated with polymers [7] but generally, the interest has been on their energy absorption capacity well beyond the elastic deformation zone [8–15]. As for the elastic properties, increased flexural modulus on aluminum foam-

* e-mail: pascal.jolly@univ-poitiers.fr

Table 1. Foam properties.

Constituent material	Al	Cu	NiCr
PPI (No. of pores / inch)	8–12	27–33	27–33
Relative density (ρ_r)*	5%	5%	7.8%
Specific surface (m^2/m^3)	500	2800	2800
Average density (gr/cm^3)	0.11	0.4–0.5	0.45–0.9
Plate thickness (mm)	10	5	10
Sample mass (gr)	1.14±0.03	1.88±0.1	4.815±0.4

* In MF-PU composites, the relative density of the constituting foam (ρ_r) corresponds to the volume fraction of the metallic phase. Similarly, the porosity of the foam, which is equal to 1-ρ_r, represents the volume fraction of the filler phase when fully occupied by the latter.

polypropylene IPC (Interpenetrating Phase Composites) has been reported and, the foam pore size was found to influence this behavior [16]. The pioneering work of C. Hauser and R. Hauser in vibration damping of open-cell metal foams filled with different viscoelastic materials showed improved damping and stiffness to weight ratio of the composites [17]. S. Yin and N. Rayess [18] tested aluminum foam impregnated with silicone and RTV (Room Temperature Vulcanized) rubber on a Dynamic Mechanical Analyzer (DMA). An increase in damping and stiffness higher than the added contribution of each phase were found within 1 and 2 Hz of excitation frequency. In a recent study, Zh. Jiang et al. [19] prepared a novel multi-scale composite having a CuAlMn memory alloy skeleton and a polymer matrix which was reinforced with different carbon nanomaterials. The tested frequency was up to 200 Hz and the temperature range from −10 to 100 °C. The loss factor was found to be higher than 0.1 in all cases and the storage modulus increased almost 3 times when the polymer was introduced.

Metal foams have also been imbibed with fluids [20] where aluminum foams, containing an average of 20 and 40 pores per inch (PPI) were imbibed with water, oil, glycerol and petroleum jelly and tested in a device consisting of a base excitation − mass system. In all the cases, the damping ratio of imbibed foams increased slightly compared to the metal structure itself, and the higher values correspond to higher dynamic viscosities of the fluids. In the case of petroleum jelly, an increase in stiffness was also observed and it was reported that the dynamic properties were frequency dependent.

In this paper, the vibration damping of elastomer filled open-cell foams is presented. The polyurethane (PU) known for its high energy dissipation capacity, inferior elastic properties to open-cell metal foams, but also for its lower viscosity compared to silicone, was chosen to enhance the damping performance of the metal skeleton. The influence on the dynamic properties for different PU fillers and foam morphologies was evaluated. The optimal combination of material properties was chosen and tested in a rotor kit test bench. In this set-up the foam-PU composite is placed between the bearings and the housing and its capacity to reduce the rotor vibrations for different configurations is discussed.

2 Materials and methods

2.1 Materials

Three types of commercially available open-cell metal foams (MF) (Recemat-BV) were selected for comparison. Their properties as specified by the manufacturer are presented in Table 1. The Al foam is produced using replication/investment casting method (solid struts) while Cu and NiCr by electro-deposition techniques [21] (hollow struts). For global characterization of the material properties, cuboidal samples of 30×30 mm were cut by Wire EDM (Electrical Discharge Machining) with 5- and 10-mm thicknesses, predetermined by the initial plate size. All the samples were weighted and higher mass variation on NiCr and Cu in comparison to Al foam were measured (Tab. 1). In the same way, annular shaped samples with internal and external diameters of 22 and 30 mm were extracted from the NiCr foam to be used as bearing supports.

A total of three polyurethane (PU) rubbers served as filler materials. They were comprised of liquid components A and B which had to be mixed according to the recommended ratios. The physical properties of the PUs are summarized in Table 2.

2.2 Global characterization

To carry out the tests, a dynamic shaker (forced vibration resonant system) with base excitation was developed. To allow for dynamic testing in tension-compression simultaneously, prior to testing, the cuboidal foam sample was sandwiched between two aluminum plates and a thin layer of cyanoacrylate adhesive ($0.1 \div 0.2$ mm) is used to glue them together (Fig. 1). 3D printed parts guaranteed foam alignment as the glue solidified. In this set-up, the foam was positioned between a calibrated seismic mass and the oscillating base, which could be mounted directly to a piezoelectric actuator thanks to its high rigidity. Steady state vibrations were generated by the actuator capable of achieving 5000 Hz and excitation amplitudes up to 27 μm. The mass on top of the foam was free to vibrate in different directions which could lead to incorrect measurements when multiple resonant frequencies occur close to one

Table 2. Polyurethane properties.

Designation	PU-10	PU-20	PU-30
Shore A hardness	10	20	30
Specific gravity	1	1	1.03
Cure time at 25 °C (hours)	24	24	16
Mixed viscosity (cps)	3100	1000	750

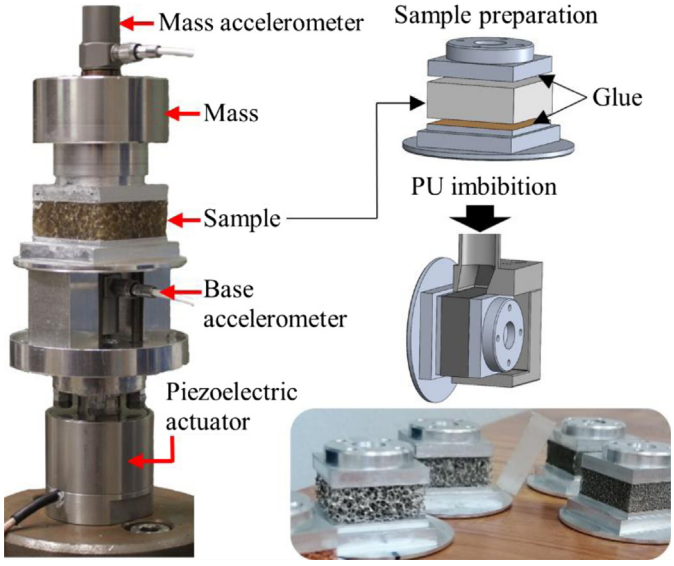

Fig. 1. Sample preparation and testing set-up for global characterization of elastic and damping properties of foams and foam-polyurethane composites.

another. To avoid this, the choices for the design of the system were made so that a wide range of frequencies was available around the compression/tension mode shape without the interference of flexural and torsional vibrations. Also, to remain within the elastic range of the material and to avoid large tensile forces, the maximum compressive/tensile amplitude (reached at the resonance frequency) was limited at $2 \div 3\,\mu m$.

The performance of viscoelastic materials is usually expressed through their dynamic modulus of elasticity $E^*_\omega = E_\omega \quad (1 + i \quad \delta_{E_\omega})$, where E_ω is the elastic (or storage) modulus, δ_{E_ω} is the loss factor and ω index signifies frequency dependency. These properties were identified using the vibration transmissibility for the foam, PU and foam-PU composites [22]. It is defined as the ratio of the mass displacement to base excitation amplitudes, $|x_{Mass}|$ and $|x_{Base}|$. In a single degree of freedom system, the transmissibility T can be written as:

$$T = |\frac{x_{Mass}}{x_{Base}}| = \frac{\sqrt{\left(1 + \delta^2_{E_\omega}\right)}}{\sqrt{\left(1 - \omega^2 \frac{hM}{AE_\omega}\right) + \delta^2_{E_\omega}}}. \quad (1)$$

In equation (1), ω is the angular speed, h and A stand for sample height and cross-sectional area and M is the seismic mass. For low-damping materials, as expected for the foams due to their metallic constituent, E_ω and δ_{E_ω} vary little with frequency. Thus, the above equation was simplified by considering E_ω and δ_{E_ω} as constants. These two parameters were then found by applying a least square fit on experimental data. Four different masses were also used with 0.238, 0.338, 0.454 and 0.554 kg each in order to evaluate the variation of the dynamic properties for different preloads and frequencies. Once the tests without the filling polyurethane (PU) were carried out, the foam samples were imbibed and retested. Before imbibition, the components A and B of the PU were carefully mixed and degassed in a vacuum chamber for about 3–4 minutes. Then, with the help of a 3D printed mold, the polymer was infiltrated under gravity into the foam for about 15–20 min inside a vacuum chamber, at 1 mbar (Fig. 1). The curing was done at room temperature for 24 h. In the same way, three different polyurethane-only samples of $30 \times 30 \times 10$ mm were prepared in order to characterize their behavior separately. Since polyurethane sticks firmly to the Al plates, no gluing was necessary in these cases. The hardness of the PUs was verified on a Shore A durometer indentation test to assure complete polymerization. In the case of high-damping materials like PU, the frequency dependent properties E_ω and δ_{E_ω} can be evaluated directly using equations (1)and (3) derived from the complex form of the transmissibility $T^* = T^{i\varphi} = T(\cos\varphi + i\sin\varphi)$ with φ being the phase angle between mass and base accelerations [23]:

$$E_{a\omega} = \frac{hM\omega^2}{A} \frac{Im(T)^2 + [Re(T) - 1]\cdot Re(T)}{Im(T)^2 + (Re(T) - 1)^2} \quad (2)$$

and,

$$\delta_{E_\omega} = \frac{Im(T)}{Im(T)^2 + [Re(T) - 1]\cdot Re(T)}. \quad (3)$$

2.3 Foam morphology

X-ray microtomography (μCT) scans with a resolution of 20 μm were also performed on all the foams to characterize their microstructure before the dynamic tests. This provided accurate insight on the local distribution of its internal features. The main geometric properties defining the foam are its relative density (the fraction of a given volume occupied by the solid material), and the cell size

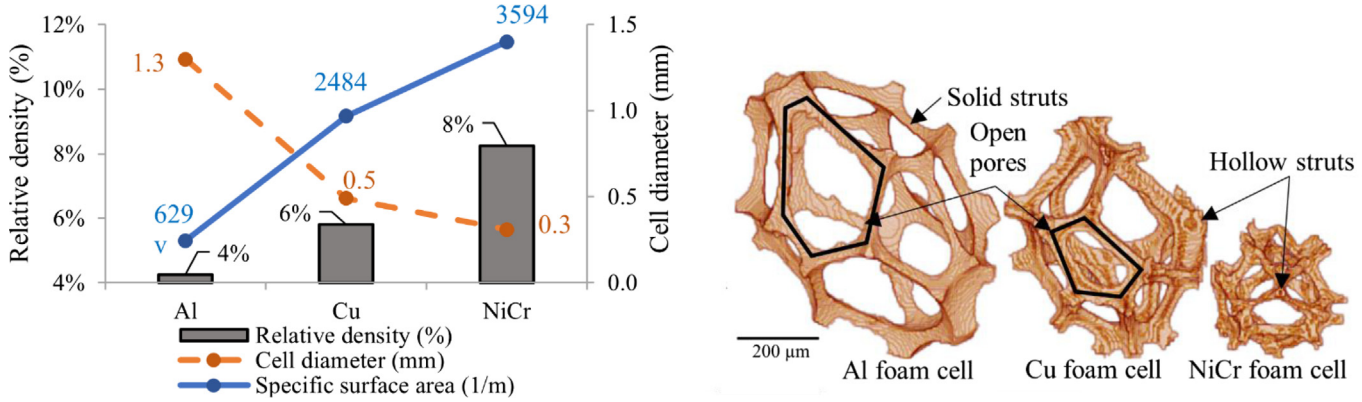

Fig. 2. Morphological properties of Al, Cu and NiCr foams. The measurements are performed in thresholded 3d images using ImageJ software.

whose measured values are presented in Figure 2. The interactions between the metal matrix and the polyurethane filler occur at the interface where the two phases meet. The size of this interface plays an important role on the behavior of the composite. This property can be described by the specific surface area which defines the total surface area per unit bulk volume. It depends on cell size and relative density, and was obtained directly from the 3D images (Fig. 2), where only the outer surface of the struts was considered for NiCr and Cu foams.

2.4 Rotor-kit test bench

A RK4 rotor kit (Bently Nevada) was used to test the annular NiCr foam samples, imbibed or not with the filler PU, and compare them with an installation without foam where the bearing was mounted directly on a rigid support (Fig. 3). The foam sample was placed between the ball bearing (Misumi TBB6900ZZ) and the housing. The test rig was equipped with two disks with mass 800 gr and 75 mm diameter each, that are mounted on a 10 mm shaft. Two types of tests were carried out using different configurations, with flexible and semi-rigid rotors. In the first case, the displacements along the shaft were monitored for rotational speeds up to 6000 RPM using 8 proximity probes (two on each plane numbered as shown on the left of Fig. 3), on a balanced system. In the second case, only hammer impact tests were performed (Fig. 3) using accelerometers. The foam imbibition was done similarly to the procedure for the cuboidal samples but a special aluminum mold machined to have the same fitting tolerances as in the bearing-housing system was used.

3 Results and discussion

The transmissibility results for two Al, one Cu and two NiCr foam samples are presented in Figure 4. At first glance, a clear difference in resonance frequency between the different NiCr samples is seen (NiCr and NiCr' in Fig. 4). As mentioned in the materials section, there was on average about 10% variation in mass for these samples. The Young's modulus of highly porous materials depends strongly on their relative density, ρ_r, thereby a dispersion in mass affects the elastic properties [24]. For two foams having the same material, the ratio of their Young's modulus E_1/E_2 can be estimated using equation (4).

$$E_1/E_2 = (\rho_{r1}/\rho_{r2})^2. \quad (4)$$

Based on this, the maximal variation on stiffness that might result due to changes in mass is found to be 11%, 17% and 61% for Al, Cu and NiCr foams respectively. As expected, the Al foam with slight variations in weight has similar elastic behavior throughout its tested samples (Al and Al' in Fig. 4). In the same figure, the existence of other mode shapes can also be observed, but they had few influence in the overall results and occurred at more than 200Hz away from the resonance peak.

The measured storage modulus and loss factor of the foams are depicted in Figures 5 and 6. They showed negligible variations with frequency and preload, so considering them as constant was a reasonable assumption. The NiCr foam was stiffer than the Al and Cu foams which have similar elastic behavior. As expected, due to their metallic constituents, the loss factor of the three foams remained small.

The transmissibility for the 30 SHA-PU, the measured storage modulus and loss factor using equations (2) and (3) are depicted in Figures 7 and 8 for a wide range of frequencies. The test was stopped after a certain frequency because the inertial effects of the sample could not be neglected anymore. Due to the intrinsic characteristics of the system with base excitation, the acceleration of the mass kept reducing with the increase in frequency and became comparable to the inertial effects on sample cross sections. In order to avoid this error and to get a rough estimation on the dynamic parameters, the same fit as for the metal matrix was applied to the transmissibility data through equation (1). It can be seen in Figure 7 that the fitted curve gave a good description of the experimental data. In the same way, the properties of the other PU samples were estimated and the overall results are summarized in Table 3.

The influence of different filler material properties on foam composites was studied through Al foam samples, which were imbibed with the 10, 20 and 30 SHA PU. This foam, having higher permeability due to its superior cell size, allowed the high viscosity PUs, especially the low

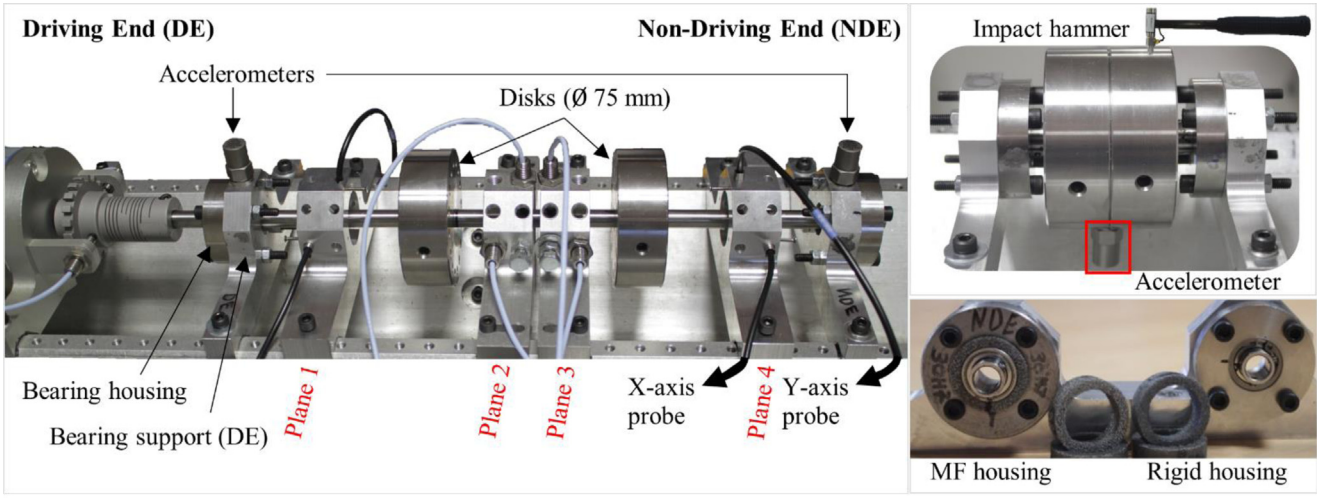

Fig. 3. RK4 rotor kit (Bently Nevada) used to obtain the vibration response of the rotor for different configurations. On the right, details about different housings and the hammer impact tests are shown.

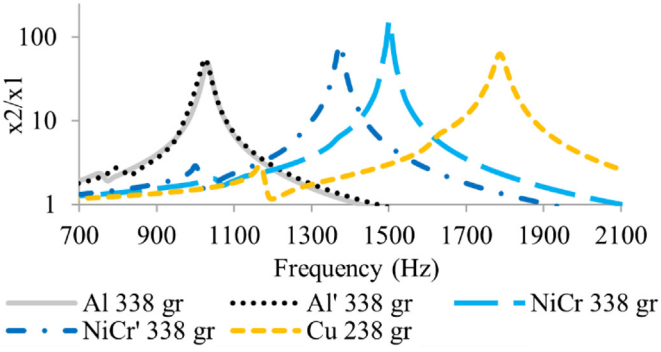

Fig. 4. Vibration transmissibility of metal foams with their respective seismic mass.

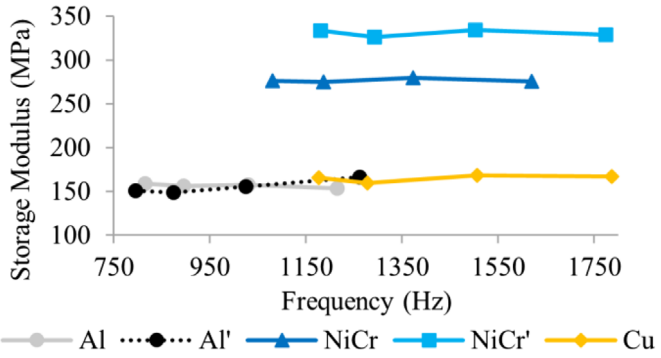

Fig. 5. Storage modulus of metal foams.

hardness ones, to penetrate easily into the foam microstructure. The storage modulus and loss factor of the foams before and after imbibition are shown in Figures 9 and 10. The inclusion of polyurethane in the metal foam matrix modified their dynamic behavior. An increase in elastic properties for the three samples is observed. Looking carefully at the evolution of the storage modulus with frequency, only a shift on the curve from the corresponding metal foam is seen, while the shape remains the same, meaning that the composite inherited the same properties as their parent metal matrix with little dependency on frequency and preload.

The storage modulus computed by adding the separate contribution of the two phases using a simplified version of the mixing law as shown in (Eq. (5)), where the foam is introduced as a separate structural unit (E_{foam}), underestimates the elastic properties of the composite E_c (see Fig. 11). The latter however, still remains within the Voigt-Reuss bounds, indicating a mutual restriction in the deformation of the constituting phases. In order to evaluate this effect, in equation (5) an extra component was added, $E_{MF/PU}$, and was attributed to the interactions between the metal foam and the polymer filler. $E_{MF/PU}$ was higher for the PUs with higher storage modulus (Fig. 12).

$$E_c = \overbrace{E_{foam}+(1-\rho_r)\cdot E_{PU}}^{Simplified\ mixing\ law} + \boldsymbol{E_{MF/PU}}. \quad (5)$$

The loss factor of the material on the other hand, from its definition can be expressed as in equation (6), where ε is the porosity of the foam and represents the volume fraction of the filling elastomer ($\varepsilon = 1-\rho_r$).

$$\delta_c = \delta_{foam}\cdot\frac{E_{foam}}{E_c} + \delta_{PU}\cdot\frac{\varepsilon\cdot E_{PU}}{E_c} + \delta_{MF/PU}\frac{E_{MF/PU}}{E_c}. \quad (6)$$

Supposing that the storage modulus of the interactions came purely from the reaction of the PU due to the constrained conditions inside the cellular structure, equation (6) becomes:

$$\delta_c = \frac{\delta_{foam} * E_{foam} + \delta_{PU} * \left(\varepsilon\cdot E_{PU} + E_{MF/PU}\right)}{E_c}. \quad (7)$$

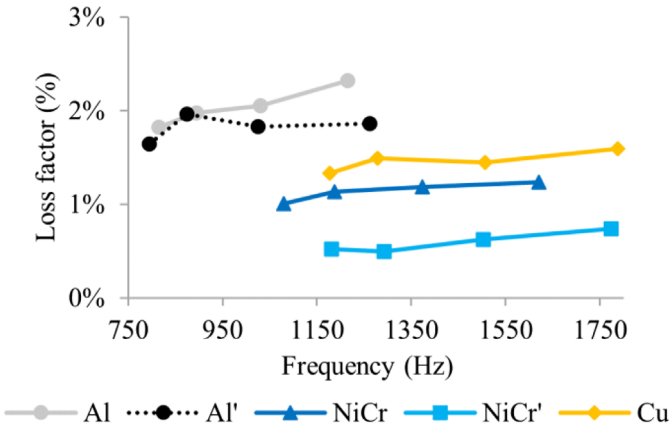

Fig. 6. Loss factor of metal foams.

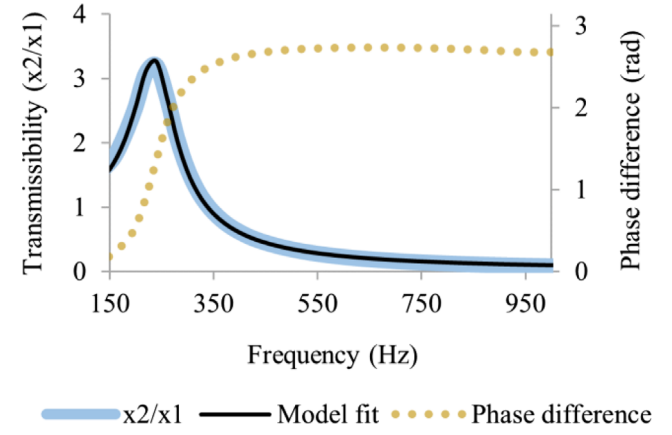

Fig. 7. Vibration transmissibility of PU-30 for a total seismic mass of 238 gr.

Table 3. PU10, PU20 and PU30 dynamic properties.

Polymer	PU10	PU20	PU30
Storage modulus (MPa)	0,86	2,94	5,8
Loss factor (%)	45	16	35

The estimated values from equation (7) agree well with the experimental data especially for the Al-PU20 and Al-PU30 (Fig. 13). This suggests that the added energy dissipation mechanism in these composites originates from the intrinsic damping of the PU phase.The 30 SHA PU performed better than the other two in terms of damping capacity and was used as a filler to study the impact of different foam microstructures on the final composite properties. Two other foam samples, Cu and NiCr were tested and imbibed using the same procedure as above. The results for Cu-PU30 and NiCr-PU30 compared to their metallic counterparts and to the previous Al, Al-PU30 are shown in Figures 14 and 15 for different frequencies. Similar to Al foam, the composite samples experience an increase in storage modulus and loss factor. Again, the evolution of the storage modulus with frequency and preload for the imbibed foams resembled to their initial metal foams. Similar effects took place concerning the loss factor, whose values for NiCr-PU30 and Cu-PU30 were close to each other and higher than for the Al-PU30 besides having the highest loss factor without filler.

Even though the same polymer was used, the overall impact in the elastic properties was greater for NiCr, followed by Cu and Al foams. The added storage modulus due to the interactions between the foam and the PU, noted as $E_{MF/PU}$, is dependent on the originating foam as depicted in Figure 16. The surface area of the metallic phase surrounding the filler material was higher for microstructures with higher specific surface area resulting in a more constrained PU, and thus its contribution on the elastic properties for the tested composites was the highest for NiCr foam. Also, the difference between Cu-PU30 and Al-PU30 which had similar elastic behaviors before PU imbibition, reflects the importance of the foam morphology over the influence induced by the varying base materials of these foams.

The predicted loss factor using equation (7), while considering only the PU as responsible for the increase in storage modulus, yielded a good approximation for the energy dissipation capacity even in the case of different metal foams (see Fig. 17).

Equation (8) defines the damping coefficient C_{eq} (or equivalent viscous damping). The product $E \cdot S$ is the highest for the NiCr-PU30 and thus the NiCr foam was used for further testing in the rotor kit test bench.

$$C_{eq} = \frac{E \cdot \delta}{\omega}. \tag{8}$$

The stiffness of the annular samples was estimated numerically using finite element analysis where the Young's modulus of the material was taken as the mean value of the storage modulus from the previous tests. Based on these results only a flexible and a semi-rigid shaft configuration could be tested experimentally. Two different housings were used to mount the ball bearings. The first one allowed for a rigid connection to the supports while on the second one the foam sample laid between the bearing outer race and its housing, so that the load on the support was transmitted through the metal foam or metal foam-PU composite (see Fig. 3). In this set-up, the bearings were placed 33 cm apart and the disks were 11 and 22 cm away from the bearing on the driving end side. The first test was run with a rigid coupling to characterize the rotor response without foam. The frequency response was obtained for rotational speeds up to 6000 rpm (100 Hz) with displacement data recorded at constant speeds for every increment of 25 rpm. The main vibration amplitudes were found within the synchronous frequencies, showing two resonance peaks at 41.6 and 48.3 Hz (see Fig. 18).

These peaks correspond to different vibration planes showing elliptical orbits, almost orthogonal to one another, indicating a highly anisotropic stiffness behavior of the

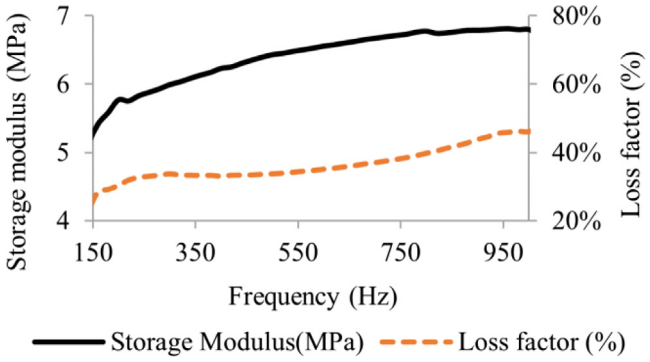

Fig. 8. Storage modulus and loss factor of PU-30 using a 238-gr seismic mass.

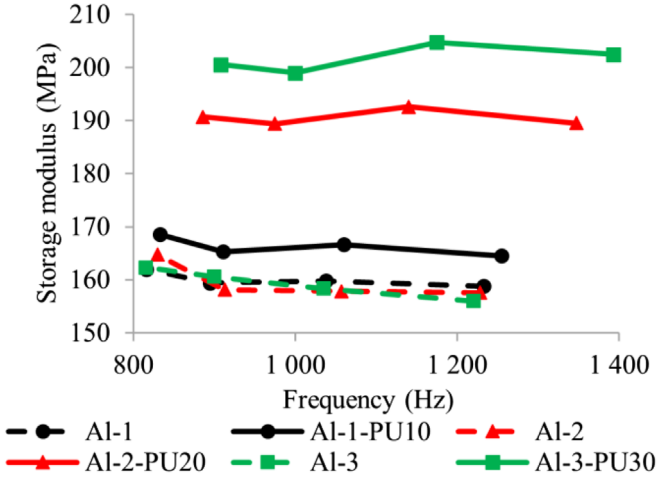

Fig. 9. Storage modulus of Al metal foam and their combination with different filler PU.

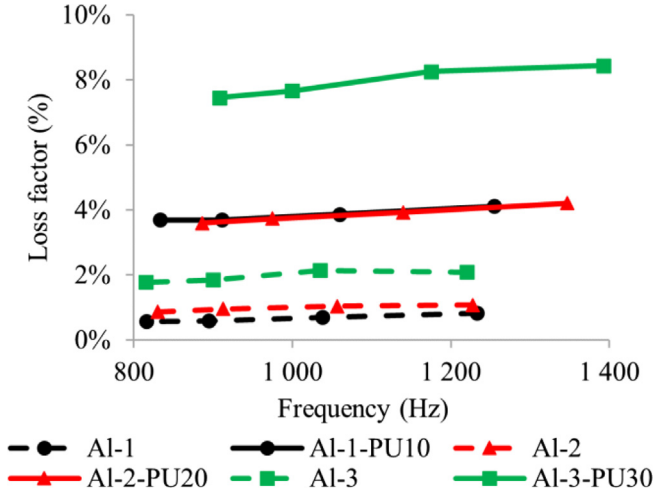

Fig. 10. Loss factor of Al metal foams and their combination with different PU.

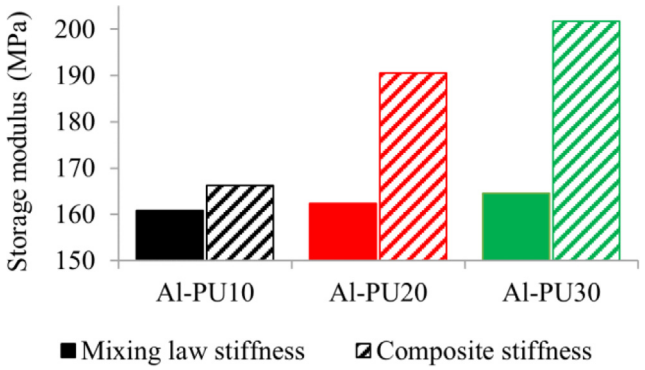

Fig. 11. Complex modulus of composites predicted by mixing law vs experimental measurements.

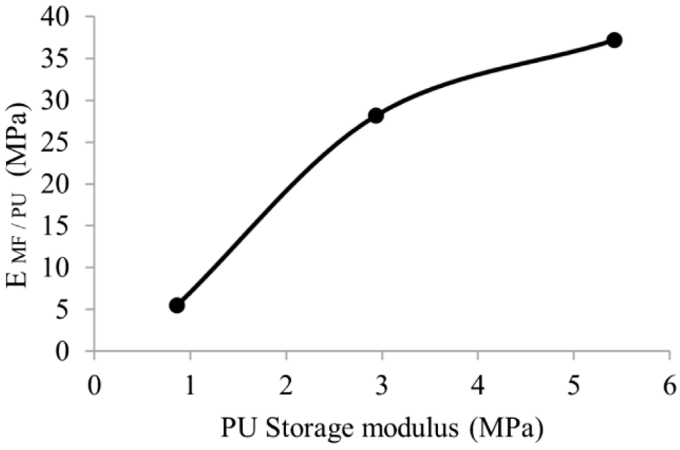

Fig. 12. Variation of storage modulus increase for different PU properties.

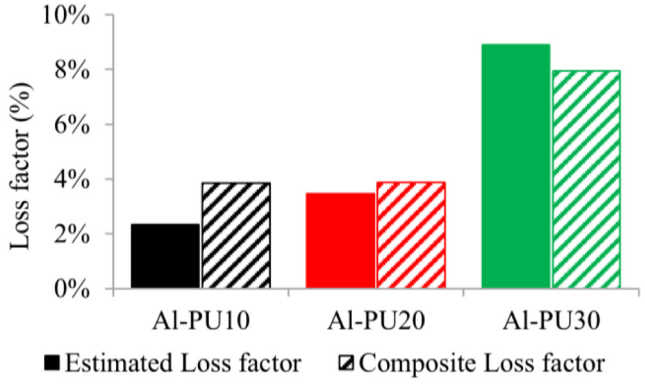

Fig. 13. Estimated loss factor of Al-PU composites considering only the PU as responsible for the increase of storage modulus.

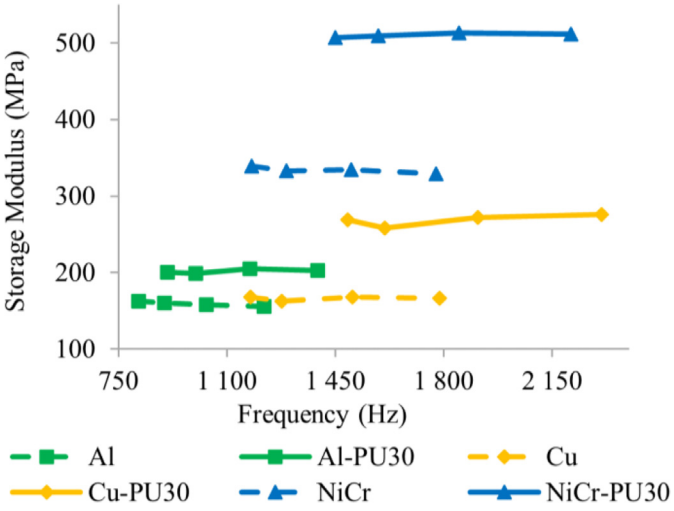

Fig. 14. Storage modulus of Al, Cu and NiCr foams and their composites formed using the 30SHA hardness PU as filler.

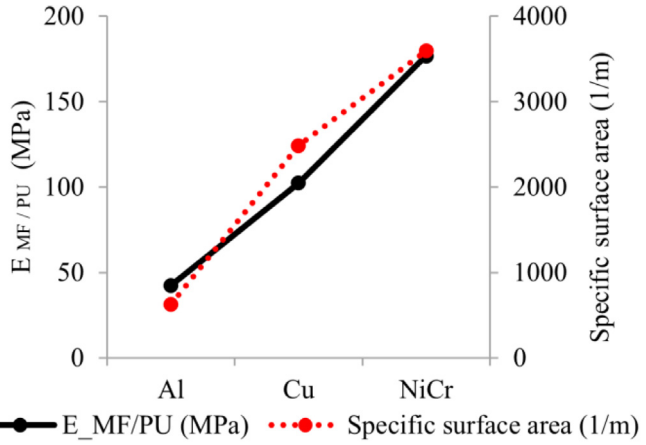

Fig. 16. The increase in complex modulus vs foam specific surface area.

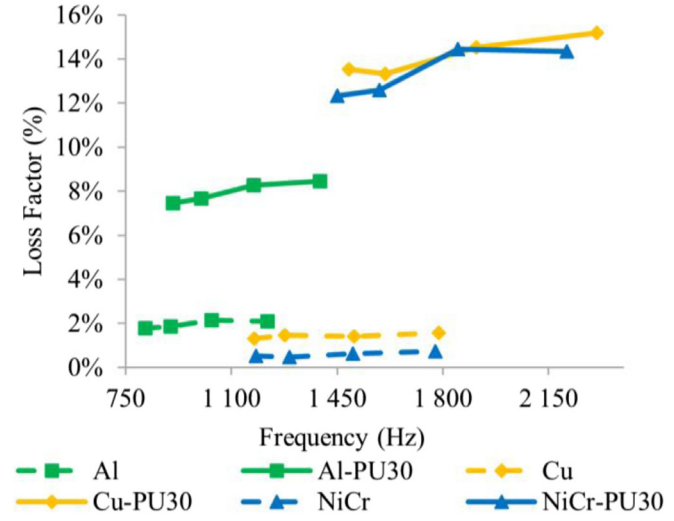

Fig. 15. Loss factor of Al, Cu, and NiCr foams and their composites formed using the 30SHA hardness PU as filler.

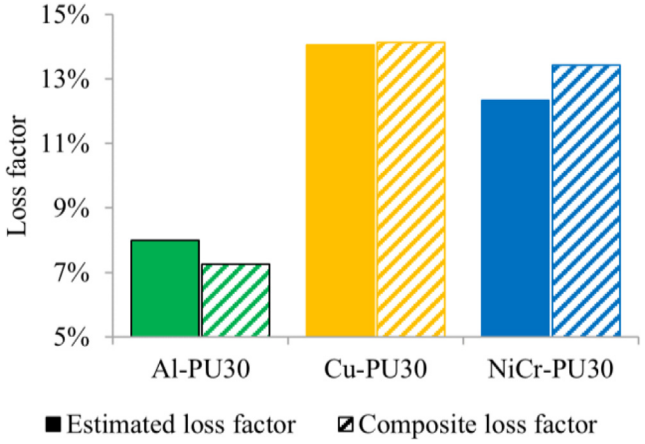

Fig. 17. Estimated loss factor of different metal foam composites based on experimental measurements for complex modulus.

bearings. The variation of the synchronous amplitudes from the middle of the shaft to its ends confirms the presence of a bending mode shape. In such configurations, with flexible shafts, most of the elastic energy is maintained in the shaft flexural mode and unsignificant energy dissipation can occur at the bearings.

The tests with metal foam were run on two pairs of samples for multiple mounting/unmounting of the foam whose bounding curves are plotted in Figure 19. Due to the high rigidity of the foam relative to the shaft, the response of the rotor after the introduction of the foam rings was still dominated by the bending mode, and as expected, the results were overall similar to the installation without them. A slight decrease of the peak amplitudes is however seen compared to the previous rigid coupling, but this was attributed to the use of two different housings and especially the influence on the foam-bearing contact from mounting/unmounting of the system. Later, one pair of the foams was imbibed with PU30 and other tests were carried out. Even in this case the difference was not significant and the influence of the MF or the MF-PU composite on the resonant amplitudes of the rotor were negligible.

To achieve efficient damping at the bearings a cylindrical mode shape is usually preferred, because the amplitude of the vibrations at the supports can be reduced by adding external damping on the bearing elements. Even though high porosity metal foams compared to non-porous materials tolerate higher elastic strains, to have an optimal stiffness for a given application and to remain within the elastic range of the material, careful design is required, considering both system and foam properties. In the current study, such an approach was sought through the

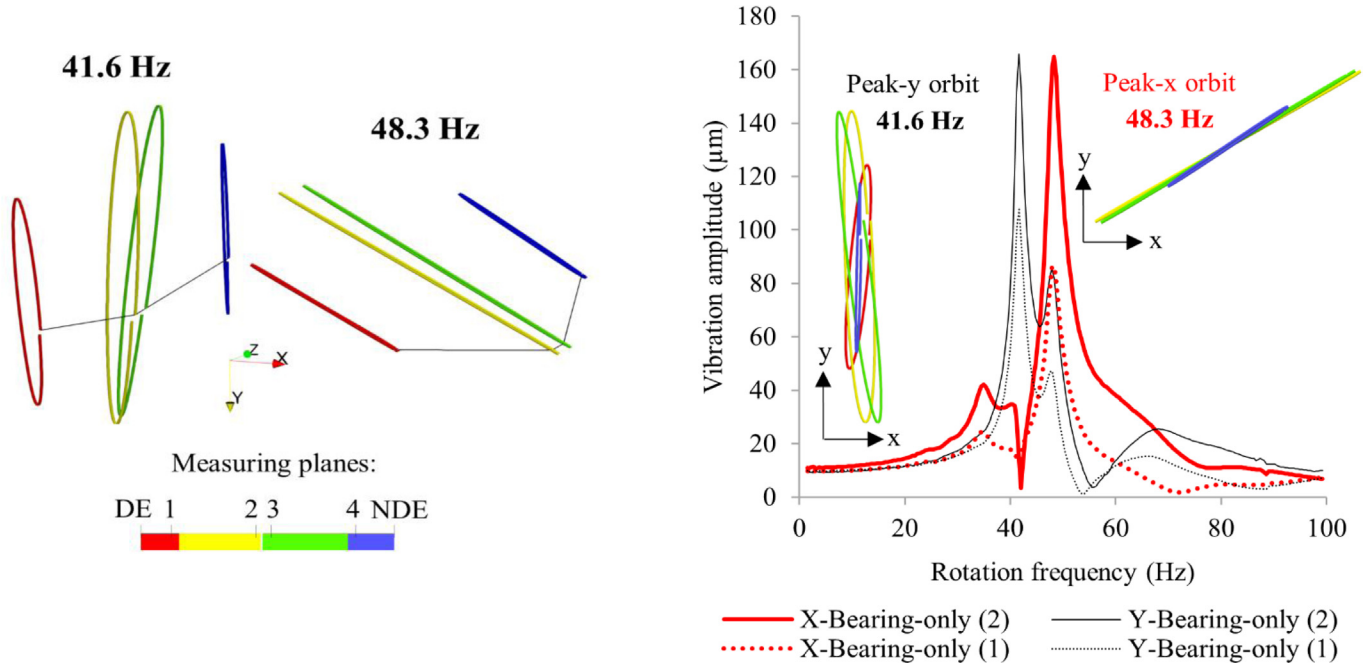

Fig. 18. Synchronous vibration response of the rotor for bearing only configuration. The measurement curves correspond to planes 1 and 2 on the DE side.

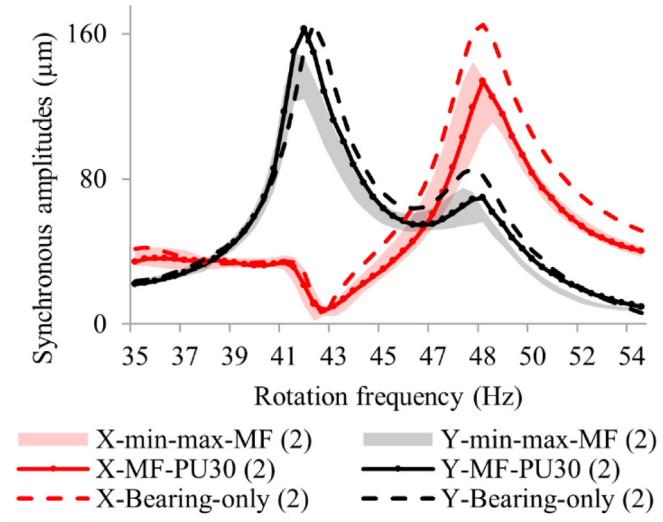

Fig. 19. Vibration response for rigid coupling, foam and foam-PU composites.

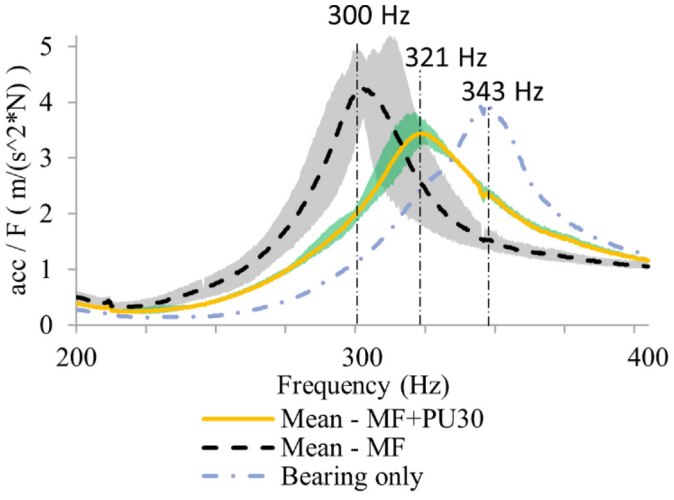

Fig. 20. Transfer function for rigid coupling, metal foam and metal foam-PU composites.

semi-rigid shaft configuration in an attempt to find a proper combination of foam and shaft stiffnesses, so that higher strains occur on the supporting foams. In this configuration, the bearings were found at a distance of 7.2 cm and the disks were placed on its center (see Fig. 3). The resonance frequency was found higher than the maximal motor speed, so only hammer impact tests were performed with an accelerometer attached below the disks (y-direction). The transfer function, defined as the ratio of the amplitudes of the acceleration and the exciting force for every excitation frequency on the excited range, was used to evaluate the stiffness and the damping of the rotor supported on bearing only, foam and foam/PU composite. The tests for the foam and for the composite were carried out for multiple unmounting/mounting of the samples and the minimal and maximal range of the results are shown in Figure 20. The tests for NiCr foam resulted with the lowest resonance frequency. Also, for this foam, a higher peak value on the transfer function compared to the rigid coupling was measured, indicating that the compression of the foam was now participating on the rotor vibration amplitudes. For the composite foam, the resonance

Table 4. Modal damping of the rotor for different configurations.

Configuration	Modal damping
MF	4.7%
MF-PU	5.9%
Bearing only	4.2%

frequency was found between the metal foam and the rigid coupling, showing that the rotor still remained in a semi-rigid condition and vibration damping could be achieved through the composite at the bearing locations. To evaluate the damping performance for the three tested scenarios, the modal damping was computed using the half bandwidth method (Tab. 4). The results affirm that the NiCr-PU30 has the highest energy dissipation capability.

4 Conclusions

Open-cell metal foams imbibed with polyurethane provide better elastic and energy dissipating capabilities than their metallic counterparts. Its final properties can be adjusted by varying the filler material or the foam microstructure.

The storage modulus and the loss factor of the tested composites were greater than the added contribution of both phases taken separately. Foam morphology played an important role in this behavior and it was shown that the increase in performance was more significant for foams with higher specific surface area.

The tests on the rotor kit carried out using a flexible shaft configuration showed no significant difference on the vibration amplitudes of the rotor between the foam, foam composites and the bearing-only set-up for rotational speeds up to 100 Hz. On the other hand, with a semi-rigid shaft the foam composites resulted with the highest energy dissipation capacity highlighting the potential of these materials. However, further investigations are required to provide an optimal combination of properties for a given application.

Funding

This work was supported by the ANR SOFITT project, grant ANR-19-CE05-0005 of the French Agence Nationale de la Recherche.

Conflicts of interest

The authors have no relevant financial or non-financial interests to disclose.

Data availability statement

The data that support the findings of this study are available from the corresponding author upon reasonable request.

Author contribution statement

All authors were involved in the tests design and execution as well as discussion of the results. Conceptualization A.L.; writing original draft preparation A.L.; validation, review and supervision P.J., J.B. and P.D. All authors have read and agreed to the published version of the manuscript.

References

[1] M. Zarzour, J. Vance, Experimental evaluation of a metal mesh bearing damper, ASME J. Eng. Gas Turbines Power **122**, 326–329 (2000)
[2] H. Ao, H. Jiang, W. Wei, A.M. Ulanov, Study on the damping characteristics of MR damper in flexible supporting of turbo-pump rotor for engine, in *1st International Symposium on Systems and Control in Aerospace and Astronautics* (2006). pp. 5–622
[3] X.Y. Zheng, Z.Y. Ren, H.B. Bai, Z.B. Wu, Y.S. Guo, Mechanical behavior of entangled metallic wire materials-polyurethane interpenetrating composites, Defence Technol. 2214–9147 (2022)
[4] L. San Andrés, T.A. Chirathadam, T. Kim, Measurement of structural stiffness and damping coefficients in a metal mesh foil bearing, ASME. J. Eng. Gas Turbines Power **132**, 032503 (2010)
[5] E.M. Al-Khateeb, J.M. Vance, Experimental evaluation of a metal mesh bearing damper in parallel with a structural support, ASME **4**, GT-0247 (2001)
[6] M. Yanhong, Z. Haixiong, D. Zhang, J. Hong, Experimental investigation on dynamic mechanical behavior of the elastic ring support with metal rubber, ASME **4B**, IMECE-62739 (2013)
[7] A. Chaturvedi, Recent developments in the field of metal foam-polymer hybrid materials: a brief overview, J. Metals Mater. Minerals **28**, 136–140 (2018)
[8] H.F. Cheng, F.S. Han, Compressive behavior and energy absorbing characteristic of open cell aluminum foam filled with silicate rubber, Scr. Mater. **49**, 583–586 (2003)
[9] J.L. Yu, J.R. Li, S.S. Hu, Strain-rate effect and microstructural optimization of cellular metals, Mech. Mater. **38**, 160–170 (2006)
[10] Y. Liu, X.L. Gong, Compressive behavior and energy absorption of metal porous polymer composite with interpenetrating network structure, Trans. Nonferrous Metals Soc. China **16**, 439–443 (2006)
[11] D. R.A. Cluff, E. Shahrzad, Compressive properties of a new metal-polymer hybrid material, J. Mater. Sci. **44**, 1573–4803 (2009)
[12] M. Vesenjak, L. Krstulović-Opara, Z. Ren, Characterization of irregular open-cell cellular structure with silicone pore filler, Polym. Test. **32**, 1538–1544 (2013)
[13] I. Duarte, M. Vesenjak, L. Krstulović-Opara, Z. Ren, Crush performance of multifunctional hybrid foams based on an aluminium alloy open-cell foam skeleton, Polym. Test. **67**, 246–256 (2018)
[14] Sh. Liu, A. Li, P. Xuan, Mechanical behavior of aluminum foam/polyurethane interpenetrating phase composites under monotonic and cyclic compression, Composites Part A **116**, 87–97 (2019)

[15] S.C. Pinto, P.A.A.P. Marques, M. Vesenjak, R. Vicente, L. Godinho, L. Krstulović-Opara, I. Duarte, Characterization and physical properties of aluminium foam-polydimethylsiloxane nanocomposite hybrid structures, Compos. Struct. **230**, 111521 (2019)
[16] N. Dukhan, N. Rayess, J. Hadley, Characterization of aluminum foam-polypropylene interpenetrating phase composites: flexural test results, Mech. Mater. **42**, 134–141 (2010)
[17] C. Hauser, R. Hauser, Vibration damping by metallic composite foams, in *9th Structural Dynamics and Materials Conference* (1968). pp. 1968–339
[18] S. Yin, N. Rayess, Characterization of polymer-metal foam hybrids for use in vibration dampening and isolation, Proc. Mater. Sci. **4**, 311–316 (2014)
[19] Z. Jiang, F. Wang, J. Yin, S. Gong, Z. Dai, Y. Pang, Y. Xiong, Z. Zhu, Z. Li, Vibration damping mechanism of CuAlMn/polymer/carbon nanomaterials multi-scale composites, Composites Part B **199**, 108266 (2020)
[20] M.J. Cops, Engineered metallic foam for controlling sound and vibration, Boston University Theses & Dissertations, 107–125 (2020). https://open.bu.edu/handle/2144/41014
[21] J. Banhart, Manufacture, characterisation and application of cellular metals and metal foams, Progr. Mater. Sci. **46**, 559–632 (2001)
[22] D. Koblar, M. Boltežar, Evaluation of the frequency-dependent young's modulus and damping factor of rubber from experiment and their implementation in a finite-element analysis, Exp. Tech. **40**, 235–244 (2016)
[23] S. Sim, K.-J. Kim, A method to determine the complex modulus and Poisson's ratio of viscoelastic materials for FEM applications, J. Sound Vibr. **141**, 71–82 (1990)
[24] L.J. Gibson, M.F. Ashby, Cellular Solids, 1st edition, Cambridge University Press, Cambridge (1998)

Cite this article as: E. Laçaj, P. Jolly, J. Bouyer, P. Doumalin, Elastic and damping characterization of open-pore metal foams filled or not with an elastomer for vibration control in turbomachinery, Mechanics & Industry **25**, 23 (2024)